

A COMPACT MULTILAYER DUAL-MODE SUBSTRATE INTEGRATED CIRCULAR CAVITY (SICC) FILTER FOR X-BAND APPLICATION

Z.-G. Zhang*, Y. Fan, Y.-J. Cheng, and Y.-H. Zhang

Fundamental Science on Extreme High Frequency Key Laboratory,
University of Electronic Science and Technology of China, Chengdu
610054, China

Abstract—A high-performance multilayer dual-mode filter is developed based on the substrate integrated waveguide circular cavity (SICC) in this paper. The filter is constructed with two circular cavities and each cavity supports two degeneration modes, which can be generated and controlled by the coupling aperture and slot located between layers. Detailed design process is introduced to synthesize an X-band dual-mode dual-layer filter. It not only has the good performances, but also reduces the circuit size much more. Moreover, it can be found that the upper side response of the filter is very steep. Good agreement is obtained between the simulated and measured results of the proposed structure.

1. INTRODUCTION

As is well known, wireless communication systems are developing gradually towards higher frequency band. Compact RF/microwave filters with low profile and high performance are required in many communication systems. For such a demand, some new planar waveguide structures called substrate integrated waveguides (SIW) have been proposed [1–8], and applied to develop many high-quality microwave wave components. SIW is a new type of dielectric-filled waveguide that is synthesized in a planar dielectric substrate with metal vias. It not only has low profile characteristic, but is easy to be integrated with planar circuitry. Due to its excellent characteristics, the SIW technology has obtained extensive concern in recent years.

Received 29 October 2011, Accepted 30 November 2011, Scheduled 6 December 2011

* Corresponding author: Zhi Gang Zhang (freemanzg@yahoo.com.cn).

Usually, SIW filters are made from rectangular cavities [1–3]. In [2], a single-cavity dual mode SIW filter with non-resonating node (NRN) is presented by etching a coplanar waveguide on the top metal layer of SIW cavity. By using an orthogonal feed line, and two slot lines for disturbing two degenerate modes, two transmission zeros are created in [3]. However, the substrate integrated waveguide circular cavity (SICC) filter is also a good choice in the design of high performance filter. It not only have the same attractiveness as classical SIW filters in terms of planar compatibility, but also presents a higher quality factor, lower loss, design flexibility [4–7]. In [4], a planar diplexer is developed based on the complementary SICC. In [5], several planar topologies of filters based on SICC are proposed. The SICC technology effectively improves the quality factor and the design flexibility.

However, the SIW technology faces a big problem, i.e., the circuit size. Accordingly, the dual-mode technology [1–15] has been introduced in the design of SIW filter to meet the requirements in size reduction and low-loss [1–8]. Here, one dual-mode SIW cavity can be referenced as two equivalent single-mode cavities, which saves the circuit size more than half. Furthermore, the multi-layer technology is another efficient way to achieve a compact circuit. Therefore, the dual-mode and multi-layer techniques can be combined together to achieve more compact circuits. More recently, it has become increasingly important because of size reduction, high quality factor, and high frequency selectivity. In [6], a Ka-band 4-pole band pass filter has been proposed using dual-mode SICC. In the cavities, the coupling via can control the coupling amount between two degenerate modes. But two additional substrate layers are added due to the vertical transition which is used for input/output port. As a result, the four layers circuit demonstrated an insertion loss of 2.95 dB and the stop-band rejection below 25 dB. In [7], a fourth-order multilayer cross-coupled circular cavity filter is proposed by using low-temperature co-fired ceramic technology (LTCC). One slot on the metal surface is introduced to suppress the spurious mode in the filter cavities. However, the above described structures exhibit poor stop-band rejection performance since only one inherent transmission zero appears at stopband. In addition, compact filters with higher selectivity and lower insertion loss are required in many applications, i.e., the diplexer and multiplexer.

In this paper, a multilayer filter with dual mode characteristic has been realized by the coupling aperture located in input/output port and the arc-shaped coupling slot etched between layers. The position of coupling aperture and slot can be used to generate two degenerate modes and also determine the coupling amount between the two modes. Meanwhile, it is possible to control the bandwidth and

the rejection level by adjusting the size and relative position of the arc-shaped slot. The proposed structure is not only very compact (without any additional layers needed), but has low insertion loss (1.9 dB), high selectivity and better stop-band rejection (> 45 dB). Moreover, it can be found that the upper side response of the filter is very steep.

2. FILTER ANALYSIS AND DESIGN

2.1. Multilayer Dual-mode SICC Filter

As shown in Figs. 1(a) and (b), there are two substrate layers. The input and output ports are distributed in the first and second layers, respectively. Two dualmode cavity resonators are coupled through arc-shaped coupling slot in metal layer 2.

In these figures, α is the angle between the coupling slot and input/output port, R is the radius of the SICC, W_S is the width of the coupling slot, θ is the central angle of the coupling slot, W_C is the width of the coupling aperture, W_g is the width of the input and output SIWs.

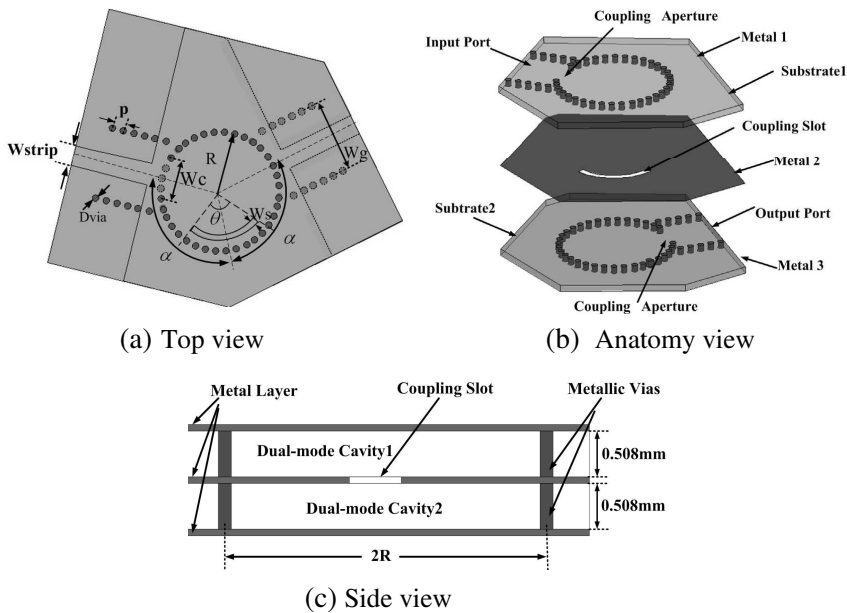


Figure 1. Proposed dual-mode SICC filter with two layers.

2.2. Dual Mode SICC Principle

As is well known, the dual-mode phenomenon exists in many cavities including SICC and can be generated only when the position of coupling slots aren't co-axial [4]. Compared with the rectangular cavity, the SICC's are more suitable to be used as dual-mode cavities due to smooth inner surfaces. For a SICC, the degeneration modes are two orthogonal modes: the horizontal TM_{110} mode and the vertical TM_{110} mode. These two degeneration modes have the same resonant frequency. The resonant frequency of mode for circular cavity with solid wall can be calculated by [19]:

$$f_{mnp} = \begin{cases} \frac{c}{2\pi\sqrt{\mu_r\epsilon_r}} \sqrt{\left(\frac{\mu'_{mn}}{R}\right)^2 + \left(\frac{p\pi}{\Delta h}\right)^2} & TE_{mnp} \\ \frac{c}{2\pi\sqrt{\mu_r\epsilon_r}} \sqrt{\left(\frac{\mu_{mn}}{R}\right)^2 + \left(\frac{p\pi}{\Delta h}\right)^2} & TM_{mnp} \end{cases} \quad (1)$$

where μ_r and ϵ_r are relative permeability and permittivity of the filling material, μ_{mn} and μ'_{mn} is the n th roots of m th Bessel function of the first kind and its derivative, R is the radius of circular cavity, and c is the speed of light in free space. For $m > 0$, each m represents a pair of degenerate TM and TE modes ($\cos m\varphi$ or $\sin m\varphi$ variation). In circular cavity, TM_{110} , the second order mode, is selected as the working mode. Different directions represent different TM_{110} modes ($\cos m\varphi$ and $\sin m\varphi$ variation). μ_{mn} is 3.832 for the TM_{110} mode. Therefore, the corresponding resonant frequency of TM_{110} is:

$$f_{110} = \frac{c}{2\pi\sqrt{\mu_r\epsilon_r}} \cdot \frac{3.832}{R} = \frac{0.61c}{R\sqrt{\mu_r\epsilon_r}} \quad (2)$$

Then, the radius of the SICC can be obtained:

$$R = \frac{0.61c}{f_{110}\sqrt{\mu_r\epsilon_r}} \quad (3)$$

The solid wall is replaced by metallic vias to form SICC under the guideline of [5–7]. The size and spacing of metallic vias are chosen to prevent electromagnetic field leakage at the desired resonant frequency and within the manufacturing limits [16–18]. Consequently, using (3), the initial dimensions of the cavity can be determined for a desired resonant frequency with the TM_{110} mode and optimized by a full-wave simulator.

Figure 2 shows electrical fields of TM_{110} mode in a SICC cavity. There are two orthogonal degeneration modes, which can be used to realize a dual-mode filter.

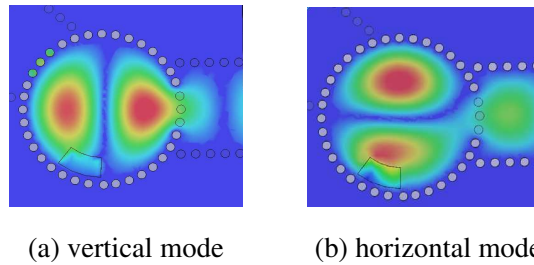


Figure 2. The E -field distribution of the TM_{110} degenerated modes.

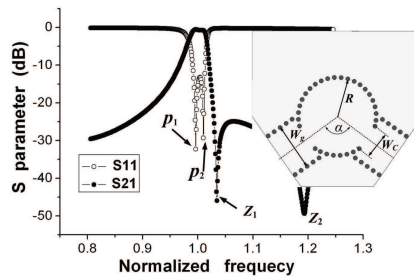


Figure 3. Response of dual-mode SICC filter with single circular cavity.

2.3. Coupling Slot

As shown in Fig. 3, two poles and two transmission zeros can be found in the response of a dual-mode filter with single circular cavity. Two poles below the zero Z_1 are denoted as P_1 and P_2 , respectively, which can be used to control the bandwidth of the passband. The first zero near the passband is denoted as Z_1 which is approximately equal to the eigenfrequency of the TM_{110} mode.

Being so close to the passband, zero Z_1 is very helpful to realize a steeper upper side response. The space between the zero Z_1 and pole P_2 decides the rolloff slope in the transition band. The coupling slot size determines the position of the first zero and then decides the slope of the upper side response. Fig. 4 illustrates varying of poles, zero for the TM_{110} mode when the coupling slot size W_S and θ are changed.

As shown in Table 1, the coupling increases when the slot size is increased. As such, it is possible to control the bandwidth and the rejection level. When the slot size is changed, the position of P_1 , P_2 and Z_1 is also modified in frequency because the amount of reactance

Table 1. Relative bandwidth change with θ and W_s .

θ (deg)	δ_{pz}/f_0	$\Delta f/f_0$ (%)	W_s (mm)	δ_{pz}/f_0	$\Delta f/f_0$ (%)
30	0.025	3	0.3	0.028	2.9
40	0.04	3.6	0.7	0.042	3.4
60	0.085	3.8	0.8	0.045	3.5

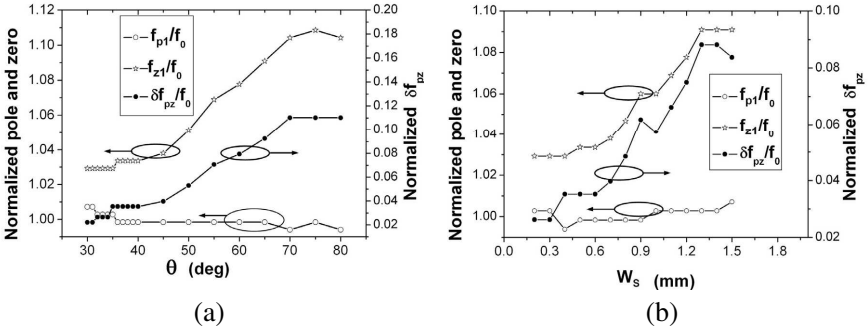


Figure 4. Variation of poles, zero and the distance between pole and zero with W_s or θ . Where, $\delta f_{pz} = f_{z1} - f_{p2}$, f_0 is the eigenfrequency of mode TM_{110} . (a) Variation of P_1 , Z_1 and δf_{pz} with respect to θ , $W_s = 0.4$ mm. (b) Variation of P_1 , Z_1 and δf_{pz} with respect to W_s , $\theta = 34^\circ$.

introduced by the slot has been changed. As shown in Fig. 4, the distance between the zero Z_1 and pole P_2 decreases evidently with the width of coupling slots W_s or θ decreased. Meanwhile, a small change occurs in the frequency of P_1 . The steeper rolloff slope and narrower bandwidth are obtained.

Figure 5 shows the relationship between zero Z_2 and α . In addition, the other zero Z_2 is independent of eigenmodes. The distance between Z_2 and the center frequency f_0 are increased with the angle α . To suppress the undesirable spur, the angle α should be adjusted carefully to assure the second zero Z_2 over the spur. Generally, smaller α or θ corresponds to narrower bandwidth and steeper rolloff slope in transition band.

As shown in Table 2, the angle α may also affect the bandwidth. A large value of α should be chosen for a broadband filter, while a small α may be proper for a narrowband filter. From the above discussion, α determines the second zero Z_2 , which is in the stop band and close to the adjacent TM_{210} mode. The proper value of α is between 100

Table 2. $\Delta f/f_0$ change with α .

W_c/R	α (deg)	$\Delta f/f_0$ (%)
0.7	110	3.5
0.7	120	3.6
0.7	130	4.1

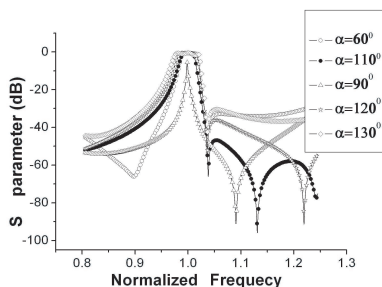


Figure 5. Relation between zero Z_2 and α . Here, operation frequency is normalized by f_0 .

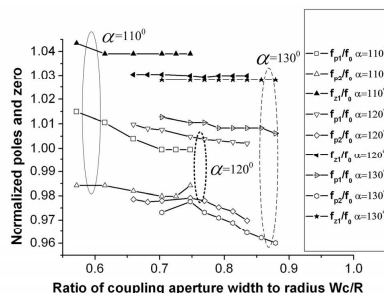


Figure 6. Variation of poles P_1 and P_2 and zero Z_1 with respect to W_c/R . Here, f_0 is the eigenfrequency of mode TM_{110} , R is the radius of the cavity.

and 130 degrees. Accordingly, the angle between the input and output ports can be controlled by changing the angle α .

2.4. External Feeding Structure

The microstrip tapered transitions are proposed to feed the SICC cavities as the input/output ports. As shown in Fig. 1, the waveguide located in input/output port can be used to suppress some undesirable response spur and improve the lower stop band characteristic. In addition, the proper parameters W_g , W_C and W_S can suppress the fundamental mode of the cavities, assure more poles not to overlap and achieve better response character in passband.

As shown in Fig. 6, for a given angle α , the proper parameter W_c/R is limited in a relatively narrow interval. Beyond the limitation, the dual-mode phenomenon may disappear and the performance is worsened. Furthermore, α also affects the bandwidth. The space between the zero and pole decides the rolloff slope in the transition band.

As shown in Fig. 7 and Table 3, the bandwidth and rolloff slope

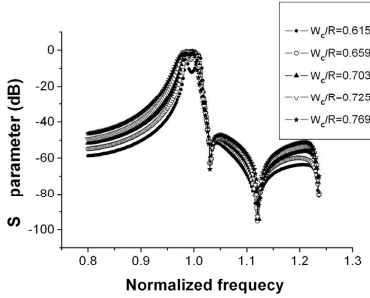


Figure 7. Variation of frequency responses with respect to W_c/R , where R is the radius of the cavity.

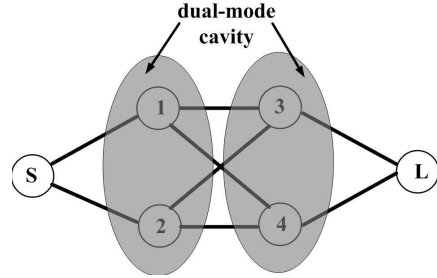


Figure 8. Coupling scheme of fourth-order dual-mode filter (gray areas show dual-mode cavities).

Table 3. $\Delta f/f_0$ change with W_c/R .

W_c/R	α (deg)	$\Delta f/f_0$ (%)	W_c/R	α (deg)	$\Delta f/f_0$ (%)
0.6	110	3.1	0.7	130	3.6
0.68	110	3.3	0.78	130	3.8
0.769	110	3.6	0.85	130	4.5

in the transition band will be affected by W_c/R for a given angle α . In general, smaller W_c/R leads to narrower bandwidth and steeper rolloff slope in the transition band.

2.5. Design Example

In our design, the center frequency and bandwidth of the filter are 10 GHz and 350 MHz, respectively. The used substrate is Rogers 5880 with relative permittivity (ϵ_r) of 2.2 and height of 0.508 mm. All the SICC here operate at TM_{110} mode. For the present design, the first step is to decide the dimensions of the cavities. According to the Formulas (2) and (3), the initial values of radius of these SICC cavities (R) should be 12.3 mm. The space between two adjacent vias (p) is uniformly arranged around 1.5 mm, thus it can satisfy the condition mentioned in part 2.2 to avoid field leakage at the desired resonant frequency. The vias in SICC are arranged with an equivalent angle between two adjacent ones.

The second step is to calculate the coupling coefficients and external quality factor. Two transmission zeros are located at upper side of the passband. The coupling scheme of the proposed dual-mode

filter is presented in Fig. 8. Resonators 1, 2 and 3, 4 represent two orthogonal degenerate modes, respectively.

Then, external quality factor Q of such a filter meeting these requirements can be extracted by the certain technique of optimization adopted in [20], and given by

$$Q_{ei} = Q_{eo} = 46.38 \quad (4)$$

In Figs. 1(a) and (b), the coupling between cavities 1 and 2 is realized by introducing an arc slot in the common wall between them. The coupling strength between two cavities depends on all of the geometrical parameters of the filter, which is described by the coupling coefficient calculated by [21]:

$$M_{i,j} = \pm \frac{f_e^2 - f_m^2}{f_e^2 + f_m^2} \quad (5)$$

where f_e and f_m are the resonant frequencies of two coupling cavities corresponding to its symmetrical plane replaced by an electric wall and a magnetic wall, respectively. From Fig. 8, we find that the source is coupled to both modes with coupling coefficients: M_{S1} and M_{S2} . M_{3L} and M_{4L} denote the coupling between load and each resonator. According to frequency responses of the dual-mode filter, a wide and deep side-band rejection can be obtained by the two transmission zeros (TZs), which is attributed to two cross coupling paths. The coupling path that generates the TZs is formed by M_{14} . In addition, M_{13} , M_{24} are the couplings between degenerate modes of different cavities.

The third step is to realize the coupling coefficients and external quality factor by suitably choosing the lengths, locations, and shapes of the coupling aperture and slot. The external quality factors are controlled by the width of the coupling aperture (W_c) and given directly by (4). The coupling between cavity 1 and cavity 2 is achieved by the slot on the common broad wall. The slot is located close to the maximum magnetic fields of the cavities. From the above discussion and the specifications, the initial geometrical parameters of slot and cavities will be determined as flowing steps:

(A). the parameters of the arc coupling slot: W_S , θ . The coupling slot size determines the position of the first zero Z_1 . According to Fig. 4 and Table 1, the initial geometrical parameters of slot will be determined to meet filter specification. One can choose the width of the coupling slot with $W_S = 0.8$ mm, the central angle $\theta = 36^\circ$.

(B). the angle between the coupling slot and input/output port: α . On the one hand, the angle α is the key factor to realize the TM_{110} degenerated modes in multilayer SICC. The dual-mode phenomenon can be easily excited by setting the angle α between 100 and 130 degrees. On the other hand, the angle α also determines the second

zero Z_2 , which is in the stop band and close to the adjacent TM_{210} mode. To achieve better stop band rejection, the distance between Z_2 and the center frequency f_0 can be decreased by selecting the smaller α . According to Fig. 5 and Table 2, the proper value of α is 110° .

(C). the width of the coupling aperture: W_C . The bandwidth and rolloff slope in the lower transition band will be affected by W_c/R . As shown in Fig. 7 and Table 3, the width of the coupling aperture will be determined as $W_c/R = 0.7$.

3. EXPERIMENT RESULTS

Now, a multilayer dual-mode SICC filter with two circular cavities is fabricated with PCB process. Fig. 9 is a photograph of the fabricated dual-mode filter.

The metallic via diameter is 0.8 mm. The space between two adjacent vias is uniformly arranged around 1.5 mm, and the width of input or output SIW is 13 mm, which can suppress the fundamental mode of the cavities. The vias in SICC are arranged with an equivalent

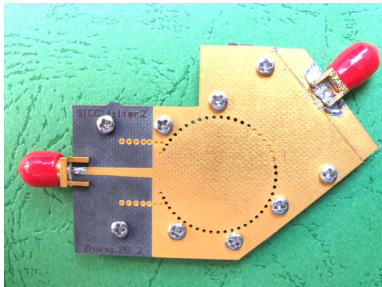


Figure 9. Photograph of the fabricated filter.

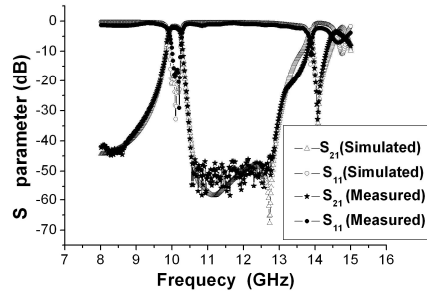


Figure 10. Simulated and measured results of the dual-mode SICC filter.

Table 4. Parameters of the fabricated filter.

D via (mm)	0.8	W strip (mm)	1.58
p (mm)	1.5	W_g (mm)	13
ϵ_r	2.2	W_c (mm)	8.2
W_S (mm)	0.7	h (mm)	0.508
α (deg)	110	R (mm)	12
θ (deg)	35		

angle between two adjacent ones. All the transition tapers from the SIWs to microstrips are the same with a length of 10 mm and widths of 2.3 and 1.58 mm at two ends.

After optimization implemented by Ansoft HFSS, the geometry parameters of the proposed filter are listed in Table 4. As shown in Fig. 10, the fabricated filter has a center frequency of 10.05 GHz with a bandwidth of 332.3 MHz. The maximum return loss of the proposed filter is 18.5 dB within the pass band and the insertion loss is about 1.9 dB. It is demonstrated that measured results agree very well with simulated ones except for a little frequency offset. The insertion loss is a little higher compared with the simulated one because of transition losses between the SMA connectors and the microstrip.

4. CONCLUSION

A novel multilayer dual-mode SICC filter has been designed, fabricated, and measured in this paper. The bandwidth and restraint outside the band can be controlled by adjusting the size of the coupling aperture and arc-shaped slot. The measured maximum return loss is 18.5 dB over pass band while the insertion loss is about 1.9 dB. Its stop band is from 10.6 to 12.8 GHz with the rejection more than 45 dB. Good agreement is obtained between the simulated and measured results of the proposed structure. This structure is very compact and well suited for the microwave and millimeter wave applications.

ACKNOWLEDGMENT

This work is supported in part by the National Natural Science Foundation of China (NSFC) under grant 61001028 and in part by Research Fund for the Doctoral Program of Higher Education of China (RFDP) under grant 20100185110014 and in part by the Fundamental Research Funds for the Central Universities under grant ZYGX2010J019.

REFERENCES

1. Deslandes, D. and K. Wu, "Substrate integrated waveguide dual-mode filters for broadband wireless systems," *RAWCON'03 Proceedings*, 385–388, Aug. 2003.
2. Shen, W., X. W. Sun, W. Y. Yin, J. F. Mao, and Q. F. Wei, "A novel single-cavity dual mode substrate integrated waveguide filter with nonresonating node," *IEEE Microw. Wirel. Compon. Lett.*, Vol. 19, No. 6, 368–370, Jun. 2009.

3. Li, R. Q., X. H. Tang, and F. Xiao, "Substrate integrated waveguide dual-mode filter using slot lines perturbation," *Electron. Lett.*, Vol. 46, No. 12, Jun. 10, 2010.
4. Tang, H. J., W. Hong, J.-X. Chen, G.-Q. Luo, and K. Wu, "Development of millimeter-wave planar diplexers based on complementary characters of dual-mode substrate integrated waveguide filters with circular and elliptic cavities" *IEEE Trans. Microw. Theory Tech.*, Vol. 55, No. 4, 776–781, Apr. 2007.
5. Potelon, B., J. C. Bohorquez, J. F. Favenec, C. Quendo, and E. Rius, "Design of Ku-band filter based on substrate-integrated circular cavities (SICCs)," *IEEE MTT-S International Microwave Symposium Digest*, 1237–1240, Jun. 2006.
6. Ahn, K. and I. Yom, "A Ka-band multilayer LTCC 4-pole bandpass filter using dual-mode cavity resonators," *2008 IEEE MTT-S International Microwave Symposium Digest*, 1235–1238, Jun. 2008.
7. Wei, Q.-F., Z.-F. Li, L.-S. Wu, W.-Y. Yin, J.-F. Mao, and L. Li, "Compact cross-coupled circular cavity filters using multilayer substrate integrated waveguide," *Electron. Lett.*, Vol. 45, No. 6, Mar. 12, 2009.
8. Hu, G., C. J. Liu, L. Yan, K.-M. Huang, and W. Menzel, "Novel dual mode substrate integrated waveguide band-pass filters," *Journal of Electromagnetic Waves and Applications*, Vol. 24, No. 11–12, 1662–1672, 2010.
9. Wang, J.-P., L. Wang, Y.-X. Guo, Y.-X. Wang, and D.-G. Fang, "Miniaturized dual-mode bandpass filter with controllable harmonic response for dual-band applications," *Journal of Electromagnetic Waves and Applications*, Vol. 23, No. 11–12, 1525–1533, 2009.
10. Zhao, L.-P., X.-W. Dai, Z.-X. Chen, and C.-H. Liang, "Novel design of dual-mode dual-band bandpass filter with triangular resonators," *Progress In Electromagnetics Research*, Vol. 77, 417–424, 2007
11. Wei, C.-L., B.-F. Jia, Z.-J. Zhu, and M.-C. Tang, "Design of different selectivity dual-mode filters with E-shaped resonator," *Progress In Electromagnetics Research*, Vol. 116, 517–532, 2011.
12. Chen, C.-H., C.-S. Shih, T.-S. Horng, and S.-M. Wu, "Very miniature dual-band and dual-mode bandpass filter designs on an integrated passive device chip," *Progress In Electromagnetics Research*, Vol. 119, 461–476, 2011.
13. Cao, W.-Q., B.-N. Zhang, T.-B. Yu, A. J. Liu, S.-J. Zhao, D. S. Guo, and Z.-D. Song, "Single-feed dual-band dual-mode

- and dualpolarized microstrip antenna based on metamaterial structure,” *Journal of Electromagnetic Waves and Applications*, Vol. 25, No. 13, 1909–1919, 2011.
14. Hu, G., Y. Chen, X. Zhao, K. Huang, and C. Liu “Novel high selective bandpass filters incorporated with quasi-lumped impedance inverters,” *Journal of Electromagnetic Waves and Applications*, Vol. 25, No. 10, 1382–1390, 2011.
 15. Hu, J. P., G. H. Li, H. P. Hu, and H. Zang, “A new wideband triple-band filter using SIR,” *Journal of Electromagnetic Waves and Applications*, Vol. 25, No. 16, 2287–2295, 2011.
 16. Cheng, Y. J., W. Hong, K. Wu, and Y. Fan, “Millimeter-wave substrate integrated waveguide long slot leaky-wave antennas and two-dimensional multibeam applications,” *IEEE Transaction Antennas and Propagation*, Vol. 59, No. 1, 40–47, Jan. 2011.
 17. Cheng, Y. J., W. Hong, and K. Wu, “Broadband self-compensating phase shifter combining delay line and equal-length unequal-width phaser,” *IEEE Transactions on Microwave Theory and Techniques*, Vol. 58, No. 1, 203–210, Jan. 2010.
 18. Xu, F. and K. Wu, “Guided-Wave and leakage characteristics of substrate integrated waveguide,” *IEEE Microw. Theory Tech.*, Vol. 53, No. 1, 66–70, Jan. 2005.
 19. Pozar, D. M., *Microwave Engineering*, 2nd Edition, Wiley, New York, 1998.
 20. Cameron, R. J., “General coupling matrix synthesis methods for Chebyshev filtering functions,” *IEEE Trans. Microw. Theory Tech.*, Vol. 47, No. 4, 433–442, Apr. 1999.
 21. Hong, J. S. and M. J. Lancaster, *Microstrip Filters for RF/Microwave Applications*, Chap. 8, 235–272, Wiley, New York, USA, 2001.